Materialia 15 (2021) 101038

Contents lists available at ScienceDirect

Materialia

journal homepage: www.elsevier.com/locate/mtla

Full Length Article

Dislocation-induced plastic instability in a rare earth containing magnesium alloy

Jie Wang[a,b], Gaoming Zhu[a], Leyun Wang[a,c,*], Qingchun Zhu[a], Evgenii Vasilev[b], Xiaoqin Zeng[a,c,*], Marko Knezevic[b,**]

[a] National Engineering Research Center of Light Alloy Net Forming, Shanghai Jiao Tong University, Shanghai 200240, China
[b] Department of Mechanical Engineering, University of New Hampshire, Durham, NH 03824, USA
[c] State Key Laboratory of Metal Matrix Composites, Shanghai Jiao Tong University, Shanghai 200240, China

ARTICLE INFO

Keywords:
Magnesium alloy
Yield phenomenon
Deformation bands
In-situ SEM/EBSD

ABSTRACT

An uncommon yield point phenomenon is observed in a Mg-1.5 wt.%Nd extrusion alloy deformed in tension. The stress-strain curve exhibits a drop at the onset of yielding, which is followed by a prolonged plateau stage prior to normal strain hardening. Localized deformation bands are observed to nucleate at the upper yield stress and propagate during the yield plateau. The yield plateau exists independent of texture and grain size of the material and shows a small dependence on strain rate. It is hypnotized that the yield point phenomenon is caused by the interactions between mobile dislocations and solute clusters. Specifically, the localized deformation at the front of deformation bands is a consequence of glide carried out by dislocations being unlocked from solute clusters by stress-strain fields from propagating bands, while dislocations away from the bands remain locked and material swept by the bands hardens.

Commonly observed plastic instabilities occurring in metals and alloys are referred to as Lüders bands and Portevine–Le Chatelier (PLC) bands [1–3]. The formation of a Lüders band is preceded by onset of yielding followed by a drop in the flow stress. The Lüders band appears as a localized event of a single band separating plastically deformed and undeformed regions that grows while accommodating the plastic strain. During the propagation stage, the nominal stress-strain curve is approximately flat. After the band has passed through the entire material the deformation proceeds uniformly with positive strain hardening. Lüders bands are often found in mild carbon steels and certain Al-Mg alloys [4–7] and rationalized by the mechanism of "dynamic strain aging". Dislocation motion away from the band is inhibited by interstitial atoms.

Plastic instabilities have been occasionally observed in Mg alloys [8,9]. The phenomena have been attributed to slip transfer across grain boundaries and deformation twinning. Moreover, deformation of many Mg alloys upon yielding in compression is carried out by profuse {102} deformation twinning and in particular twin cascades (i.e. twins in one grain stimulate twins in the neighboring grain across the grain boundary) [10–12]. Plastic deformation associated with twin cascade is often localized within some deformation bands (i.e. twin bands). Since twin cascading does not involve dislocation-twin or twin-twin intersections, it causes little strain hardening, which leads to the observed plateau in the stress-strain curves of AZ31 [10,13,14], pure Mg [9], and Mg-Zn [15]. The twin-induced plastic instability in Mg is sensitive to the texture, grain size, and strain rate.

In this paper, we report a plastic instability phenomenon in a Mg-Nd alloy that is *not* associated with twinning. An alternative interpretation is proposed based on the interaction between mobile dislocations with metastable precipitates as twins are rarely observed in the deformed microstructure. The Mg-1.5 wt.%Nd alloy was melted from pure Mg (99.99%) and Mg-90 wt.%Nd master alloy in an electrical resistance furnace under the mixed protective atmosphere of CO_2 (99 vol.%) and SF_6 (1 vol.%). The melt was on hold at 750 °C for 30 min and then poured into a preheated steel mold to solidify naturally in air. The cast billet was homogenized at 400 °C for 12 h and then cut into cylinders with a diameter of 60 mm for extrusion. The extrusions were conducted at 300 and 350 °C with a speed of 2 mm/s to produce bars with a diameter of 12 mm. The two materials are named as E-300 and E-350, respectively. Flat tensile samples with gauge dimension of 18.0 mm (L) × 3.0 mm (W) × 1.7 mm (T) were cut from the extrusion bars. The tensile axis was parallel to the extrusion direction (ED). Tensile tests were carried out

* Corresponding authors at: National Engineering Research Center of Light Alloy Net Forming, Shanghai Jiao Tong University, Shanghai 200240, China.
** Corresponding author.
E-mail addresses: leyunwang@sjtu.edu.cn (L. Wang), xqzeng@sjtu.edu.cn (X. Zeng), marko.knezevic@unh.edu (M. Knezevic).

https://doi.org/10.1016/j.mtla.2021.101038
Received 8 November 2020; Accepted 14 February 2021
Available online 24 February 2021

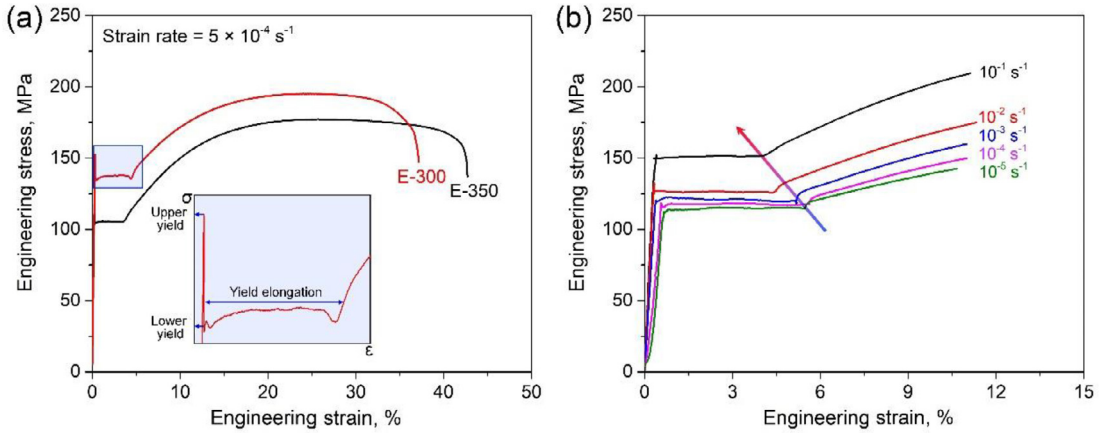

Fig. 1. (a) Tensile stress-strain curves obtained from the two as-extruded Mg-1.5 wt.%Nd alloys. (b) Tensile stress-strain curves of the E-350 alloy under different strain rates.

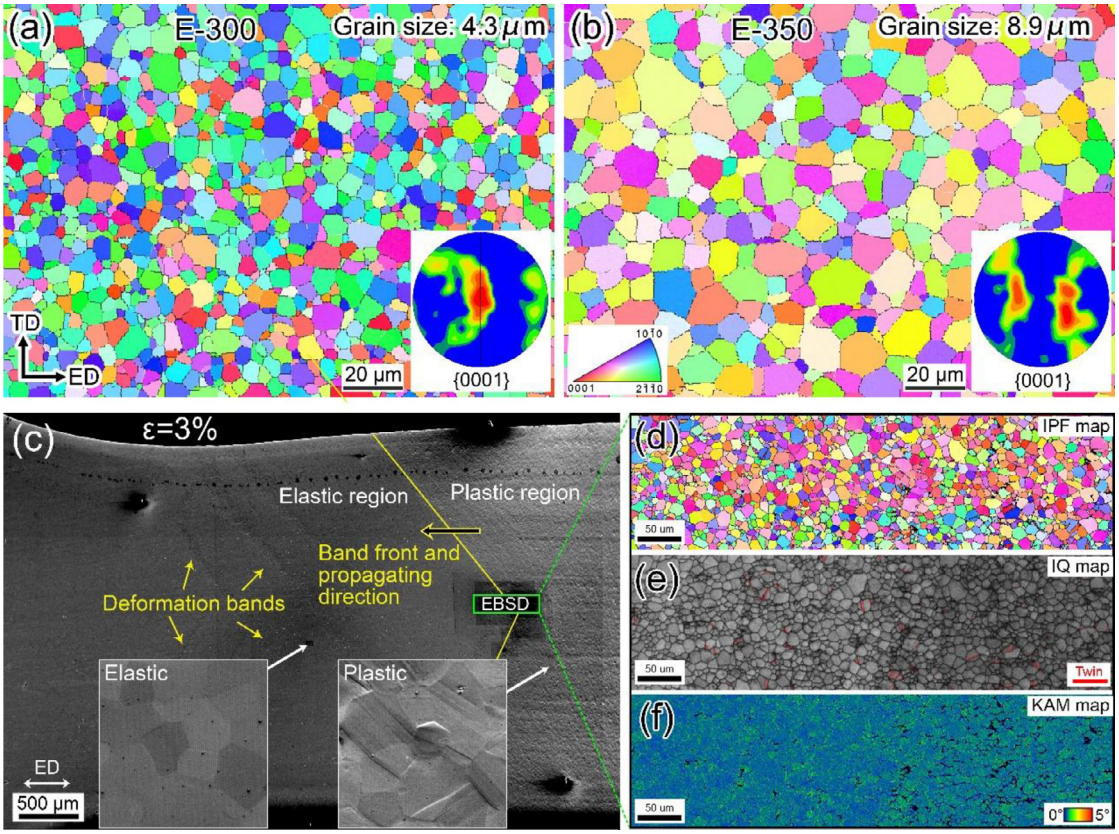

Fig. 2. Inverse pole figure (IPF) maps and pole figures of as-extruded Mg-1.5 wt.%Nd alloys, (a) extruded at 300 ˚C (named as E-300) and (b) extruded at 350 ˚C (named as E-350). Microstructures of the E-350 alloy after 3% of tensile strain: (c) Secondary electron image showing the microstructure consists of both plastic and elastic regions, (d) IPF map, (e) image quality (IQ) map, and (f) Kernel average misorientation (KAM) map of the frontier of the main deformation band marked by a green rectangular box in (a) (For interpretation of the references to color in this figure legend, the reader is referred to the web version of this article.).

using a Zwick/Roell-100 kN material test machine (Zwick USA, Kennesaw, GA, USA).

From the extrusion bar, a small-size tensile specimen with a gauge of 4.0 mm (L) × 2.0 mm (W) × 1.4 mm (T) was additionally prepared for in-situ scanning electron microcopy (SEM) and electron backscattered diffraction (EBSD) tests. Surface of the specimen was mechanically ground and then electro-polished in an ethanol-10% perchloric acid electrolyte for SEM and EBSD characterization. The electro-polishing was conducted at 30 V and 0.5 A under -25 ˚C for 150 s. The specimen was mounted in a MICROTEST 200 N (Deben, UK) module placed in a Zeiss Gemini SEM with an EBSD system (Oxford Instrument, UK). The test was paused at different strains for the acquisition of secondary electron images and EBSD data. EBSD scans were conducted at an accelerating voltage of 20 kV with a scan step size of 0.4 μm. The EBSD data were processed and analyzed using the TSL OIM Analysis 7 software (EDAX Inc). Transmission electron microscopy (TEM) was employed to characterize finer microstructure in the alloy using JEOL JEM-2100F and JEOL-ARM200 instruments. TEM samples were twin-jet electropolished in a solution of ethanol-4%perchloric acid electrolyte at 30 V and -40 ˚C, followed by ion milling.

Fig. 1(a) shows tensile stress-strain curves of the two as-extruded Mg-Nd alloys with a strain rate of 5 × 10^{-4} s^{-1}. In both materials, the

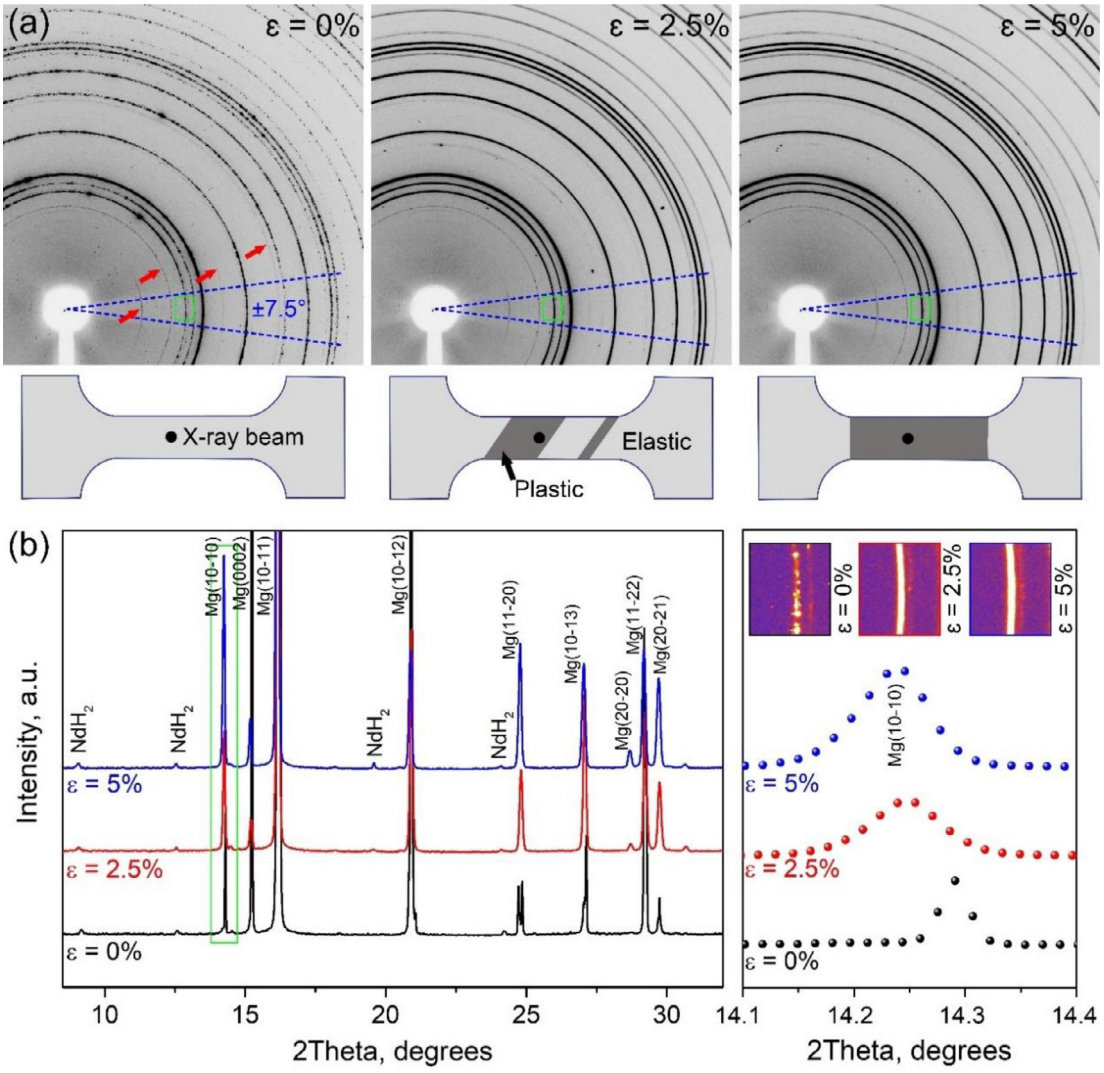

Fig. 3. (a) 2D diffraction patterns from the E-350 alloy at different tensile strains, the red arrows indicate the additional diffraction rings from NdH_2, the dotted blue lines marked the integration area. (b) Integrated diffraction profiles at different strains, the diffraction peak of Mg(10-10) is magnified (For interpretation of the references to color in this figure legend, the reader is referred to the web version of this article.).

stress-strain curves exhibit a sudden drop at the end of the elastic regime followed by a plateau stage (i.e. yield elongation). Afterwards, strain-hardening occurs. The yield elongation exhibited in two alloys accounts for ~5% tensile strain. Fig. 1(b) shows the tensile stress-strain curves of the E-350 alloy under different strain rates. When the strain rate increases from 10^{-5} to 10^{-1} s^{-1}, the lower yield strength increases from ~110 to ~155 MPa, while the yield elongation strain decreases from ~6 to ~4%. Such effect of strain rate on the mechanical behavior is similar to plain carbon steels [1,3,16,17].

Fig. 2(a) and (b) show the inverse pole figure (IPF) maps and {0001} pole figures (PF) of the investigated alloys. The two extruded Mg-Nd alloys consist of equiaxed grains with an average grain size of ~4.3 μm for the E-300 alloy and ~8.9 μm for the E-350 alloy. Both display a so-called "rare earth" texture with most grains having their c-axis being away from both TD and ED.

To understand the yield elongation phenomenon, microstructure of the E-350 alloy was characterized using SEM and EBSD after 3% tensile strain, as shown in Fig. 2(c). The material shows an inhomogeneous deformation pattern: Part of it exhibits plastic deformation while the remaining area remains elastic. There is one main deformation band spanning over the whole width of the sample. A video recorded how the deformation bands nucleate and propagate during the yield elongation is provided in the supplementary material of the paper. Apart from the main deformation band, multiple narrower deformation bands formed in the elastic region. The deformation bands were localizing and propagating with an inclination of about 45° with respect to the loading axis, which aligns with the direction of maximum shear stress. It is the nucleation and propagation of those deformation bands that causes the yield elongation phenomenon. After the deformation bands transverse the whole gauge length, strain hardening eventually takes place.

Fig. 2(d–f) show the EBSD scan results near the frontier of the main deformation band. From the IPF map, it is clear that twinning is absent in majority of grains. This finding is different from the previous studies [10,12,15], in which the plastic instability observed in Mg alloys is a consequence of profuse twinning and twin cascading. Since the tensile direction is parallel to ED, it is unsurprising that twinning is not favorable in most grains. Instead, the plastic deformation in the deformation bands is dominated by dislocation activity as evidenced by slip lines in many grains. The two insets in Fig. 2(c) compare the microstructure inside and outside the deformation band. Slip lines were extensively developed in the plastic region, while grains outside the deformation bands do not show slip lines. The KAM and IQ maps show a gradual transition from the plastic region to the elastic region. We did not ob-

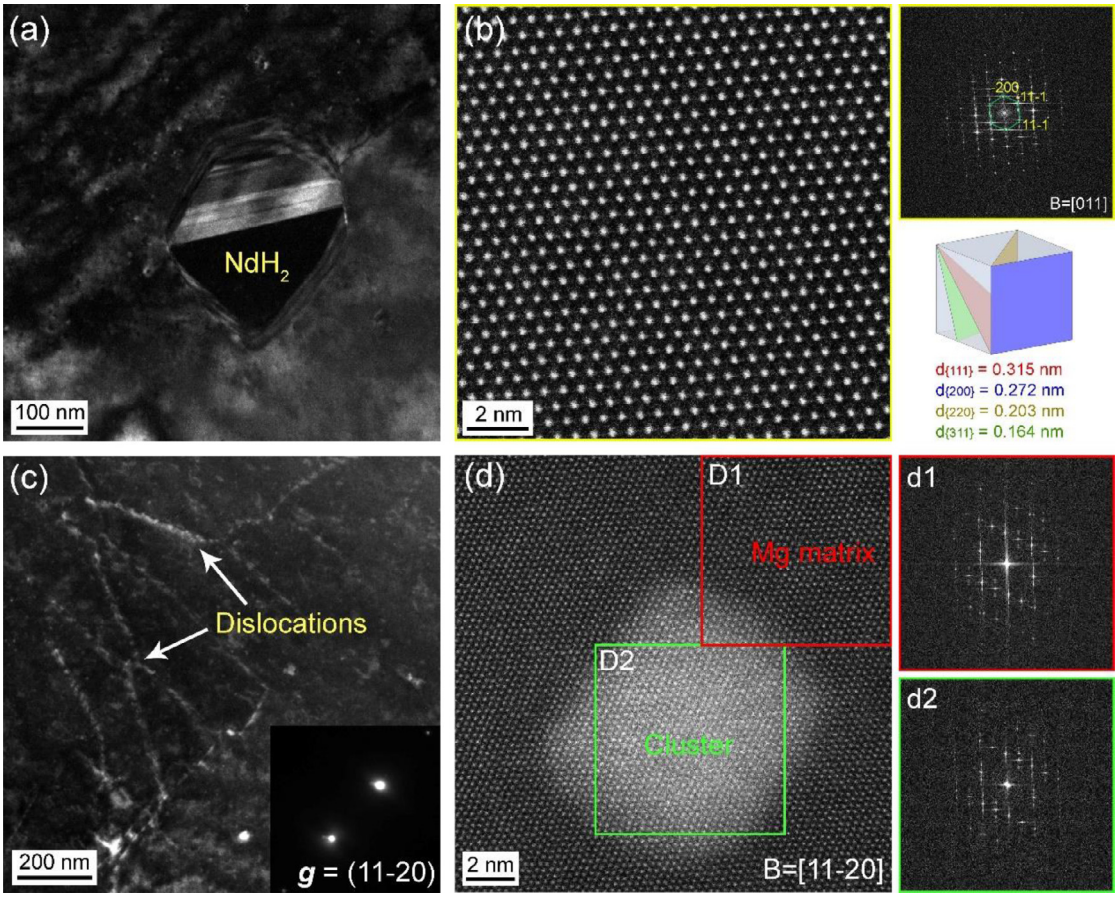

Fig. 4. TEM images showing the microstructure features in the Mg-1.5 wt.%Nd alloy. (a) Dark field (DF) image shows the morphology of NdH_2 precipitate. (b) High-resolution TEM (HRTEM) of NdH_2 precipitate and the corresponding fast Fourier transformation (FFT) pattern. (c) Initial dislocation configuration taken along the [1-100] zone axis under $\boldsymbol{g}$= (11-20) condition. (d) HAADF-STEM image showing the cluster morphology, the fast Fourier transformation (FFT) patterns obtained from the Mg matrix (marked as red square) and the cluster (marked as green square) are also presented (For interpretation of the references to color in this figure legend, the reader is referred to the web version of this article.).

serve many connected slip lines across neighboring grains within the deformation bands. Therefore, the previously hypothesized slip transfer across the grain boundaries to form deformation bands [9] is also not the case here.

To further correlate the yield point phenomenon with microstructural evolution, a synchrotron X-ray diffraction experiment was performed using three tensile specimens of the E-350 alloy. The details of the beamline, the sample dimension, and the experimental set-up can be found in Ref. [18]. The tensile tests on the three specimens were interrupted at strains of 0% (initial state), ~2.5% (in the middle of the plateau stage), and ~5% (at the end of the plateau stage), respectively. Shown in Fig. 3(a) are 2D diffraction patterns on the three specimens. Prior to deformation the alloy shows discrete diffraction spots for the rings because of the limited number of interrogated grains. After 2.5% strain, the rings became connected and all diffraction rings broaden in the radial direction as a result of dislocation activity. From 2.5 to 5% strain, the radial width of diffraction rings remains stable, indicating much slower dislocation multiplication in the plastic region. The peak broadening during the stage of plastic instability, e.g. Mg(10-10), is also illustrated in Fig. 3(b). This result confirms that plastic deformation of this Mg-Nd alloy during the yield elongation stage is caused by the localized deformation band behavior, as the regions that already developed plastic deformation kept approximately same amount of dislocations until the band extends to the entire sample. Propagation of the deformation band does not incur much strain hardening.

The original diffraction patterns in Fig. 3(a) were integrated around the tensile direction over a $\pm 7.5^{\circ}$ range. The result is shown in Fig. 3(b). In addition to Mg peaks, we also observed diffraction peaks from NdH_2, an uncommon phase for Mg alloys but observed in Nd-containing Mg alloys [19]. TEM was further conducted to examine the precipitates in the studied Mg-Nd alloy. As shown in Fig. 4(a,b), the square-shaped phase was confirmed as NdH_2. However, the NdH_2 precipitates are unlikely to cause the yield elongation phenomenon since these precipitates with size ~100 nm are coarse and cannot be effective in pinning mobile dislocations. Instead, a series of the metastable precipitates, such as GP zones/$D0_{19}$, $\beta''(Mg_3Nd)$, and $\beta'(Mg_7Nd)$ [20–24], may form in the alloy during the extrusion process, known as dynamic precipitation. Those metastable precipitates cannot be identified using XRD; instead, they can only be identified using high-angle annular dark field scanning transmission electron microscopy (HAADF-STEM) [23,24]. Fig. 4(c) shows the entangled dislocation configuration in the alloy. We further examined the material using HAADF-STEM and observed solute clusters with size of ~5 nm in the alloy, as shown in Fig. 4(d). These clusters could reduce the mean free path of dislocations and temporarily pin dislocations. A cascade-like “unpinning” of dislocations is believed to happen in the yield elongation.

In contrast to previous studies that attributed the yield elongation in Mg to twin-cascading [10, 12, 13] or slip transfer [9, 25], we now propose that the plastic instability and yield elongation in this extruded Mg-Nd alloy are caused by the dislocation behavior, specifically the interaction between initial dislocations and metastable precipitates. The

initial yielding is accompanied by rapid motion of initial dislocations. The dislocations are quickly pinned by metastable precipitates, which causes the upper yield strength. Subsequently, local stress concentration allows some dislocations to be unpinned from metastable precipitates. Since no new dislocations are generated, there is no strain hardening. Propagation of the stress concentration region/bands corresponds to the yield elongation stage, which is achieved by unlocking of dislocations at the propagating band fronts. After bands sweep throughout the material, new dislocations start nucleating and the material enters the strain-hardening stage. We acknowledge that the mechanisms pertaining to the deformation bands nucleation and propagation require further investigation. Future works will explore the nature of the yield elongation phenomenon in more detail focusing on two aspects: dislocation-precipitate interaction at atomic scale and the propagation mechanism of deformation bands.

In summary, we observed an uncommon yield point phenomenon in an extruded Mg-Nd alloy, which has not been reported among Mg alloys. The stress-strain curve of this alloy can be divided into three stages: (1) elastic extension which is terminated at a stress level known as the upper yield stress, (2) inhomogeneous deformation by the formation and propagation of localized deformation bands at a decreased stress level known as the lower yield stress, (3) typical strain hardening behavior until fracture after the deformation bands swept through the whole material. The yield elongation phenomenon is attributed to the localized deformation at the front of the bands with softening caused by the unlocking of dislocations from metastable precipitates.

Declaration of Competing Interest

The authors declare that they have no known competing financial interests or personal relationships that could have appeared to influence the work reported in this paper.

Acknowledgment

The authors are thankful for the useful discussion with Prof. Jian Wang at University of Nebraska-Lincoln. This work has been financially supported by the National Natural Science Foundation of China (Nos. 51631006, 51671127, 51825101). L.W. is sponsored by the Youth Cheung Kong Scholars Program and the Shanghai Rising-Star Program. M.K. and E.V. acknowledge support from the National Science Foundation under CMMI-1650641 grant. The authors thank beamline BL14B1 (Shanghai Synchrotron Radiation Facility) for providing the beam time and helps during experiments.

Supplementary materials

Supplementary material associated with this article can be found, in the online version, at doi:10.1016/j.mtla.2021.101038.

References

[1] E.O. Hall, Yield Point Phenomena in Metals and Alloys, Springer Science & Business Media, 2012.
[2] X.G. Wang, L. Wang, M.X. Huang, Kinematic and thermal characteristics of Lüders and Portevin-Le Châtelier bands in a medium Mn transformation-induced plasticity steel, Acta Mater 124 (2017) 17–29.
[3] R. Schwab, V. Ruff, On the nature of the yield point phenomenon, Acta Mater 61 (2013) 1798–1808.
[4] J.F. Hallai, S. Kyriakides, Underlying material response for Lüders-like instabilities, Int. J. Plast. 47 (2013) 1–12.
[5] J. Ma, H. Liu, Q. Lu, Y. Zhong, L. Wang, Y. Shen, Transformation kinetics of retained austenite in the tensile Lüders strain range in medium Mn steel, Scr. Mater. 169 (2019) 1–5.
[6] J. Zhang, Y. Jiang, Lüders bands propagation of 1045 steel under multiaxial stress state, Int. J. Plast. 21 (2005) 651–670.
[7] R. Hutanu, L. Clapham, R.B. Rogge, Intergranular strain and texture in steel Luders bands, Acta Mater 53 (2005) 3517–3524.
[8] J. Min, L.G. Hector, J. Lin, J.T. Carter, A.K. Sachdev, Spatio-temporal characteristics of propagative plastic instailities in a rare earth containing magnesium alloy, Int J Plasticity 57 (2014) 52–76.
[9] C.M. Cepeda-Jiménez, J.M. Molina-Aldareguia, M.T. Pérez-Prado, Origin of the twinning to slip transition with grain size refinement, with decreasing strain rate and with increasing temperature in magnesium, Acta Mater 88 (2015) 232–244.
[10] M.R. Barnett, M.D. Nave, A. Ghaderi, Yield point elongation due to twinning in a magnesium alloy, Acta Mater 60 (2012) 1433–1443.
[11] I. Chelladurai, D. Adams, D.T. Fullwood, M.P. Miles, S. Niezgoda, I.J. Beyerlein, M. Knezevic, Modeling of trans-grain twin transmission in AZ31 via a neighborhood-based viscoplastic self-consistent model, Int J Plasticity 117 (2019) 21–32.
[12] Y. Paudel, J. Indeck, K. Hazeli, M.W. Priddy, K. Inal, H. Rhee, C.D. Barrett, W.R. Whittington, K.R. Limmer, H. El Kadiri, Characterization and modeling of {10-12} twin banding in magnesium, Acta Mater 183 (2020) 438–451.
[13] N. Shafaghi, E. Kapan, C.C. Aydıner, Cyclic Strain Heterogeneity and Damage Formation in Rolled Magnesium Via In Situ Microscopic Image Correlation, Exp. Mech. 60 (2020) 735–751.
[14] M. Zecevic, I.J. Beyerlein, M. Knezevic, Coupling elasto-plastic self-consistent crystal plasticity and implicit finite elements: Applications to compression, cyclic tension–compression, and bending to large strains, Int. J. Plast. 93 (2017) 187–211.
[15] J. Wang, M.R.G. Ferdowsi, S.R. Kada, C.R. Hutchinson, M.R. Barnett, Influence of precipitation on yield elongation in Mg-Zn alloys, Scr. Mater. 160 (2019) 5–8.
[16] J.M. Krafft, A.M. Sullivan, in: Influence of Speed of Deformation on Strength Properties in the Post Lower Yield Stress-Strain Curve of Mild Steel, 1960.
[17] J.M. Krafft, An interpretation of lower yield point plastic flow in the dynamic testing of mild steel, Acta Metall 10 (1962) 85–93.
[18] J. Wang, L. Wang, G. Zhu, B. Zhou, T. Ying, X. Zhang, Q. Huang, Y. Shen, X. Zeng, H. Jiang, Understanding the high strength and good ductility in LPSO-containing Mg alloy using synchrotron X-ray diffraction, Metall. Mater. Trans. A 49 (2018) 5382–5392.
[19] Y. Yang, L. Peng, P. Fu, B. Hu, W. Ding, Identification of NdH2 particles in solution-treated Mg–2.5%Nd (wt.%) alloy, J. Alloys Compd. 485 (2009) 245–248.
[20] T.J. Pike, B. Noble, The formation and structure of precipitates in a dilute magnesium-neodymium alloy, J. Less Common Met. 30 (1973) 63–74.
[21] M. Hisa, J.C. Barry, G.L. Dunlop, New type of precipitate in Mg-rare-earth alloys, Philos. Mag. A 82 (2002) 497–510.
[22] K. Saito, K. Hiraga, The Structures of Precipitates in an Mg-0.5 at%Nd Age-Hardened Alloy Studied by HAADF-STEM Technique, Mater. Trans. 52 (2011) 1860–1867.
[23] B. Zhou, L. Wang, B. Chen, Y. Jia, W. Wen, D. Li, D. Shu, P. Jin, X. Zeng, W. Ding, Study of age hardening in a Mg–2.2wt%Nd alloy by in situ synchrotron X-ray diffraction and mechanical tests, Mater. Sci. Eng. A 708 (2017) 319–328.
[24] E.L.S. Solomon, V. Araullo-Peters, J.E. Allison, E.A. Marquis, Early precipitate morphologies in Mg-Nd-(Zr) alloys, Scr. Mater. 128 (2017) 14–17.
[25] X. Luo, Z. Feng, T. Yu, J. Luo, T. Huang, G. Wu, N. Hansen, X. Huang, Transitions in mechanical behavior and in deformation mechanisms enhance the strength and ductility of Mg-3Gd, Acta Mater 183 (2020) 398–407.